Predicting the flow in the floodplains with evolving land occupations during extreme flood events (FlowRes ANR project)

Sébastien Proust[1,a], Céline Berni[1], Martin Boudou[1], Antoine Chiaverini[1], Victor Dupuis[1], Jean-Baptiste Faure[1], André Paquier[1], Michel Lang[1], Sebastian Guillen-Ludena[2], Diego Lopez[2], Emmanuel Mignot[2], Nicolas Rivière[2], Loic Chagot[3], Maxime Rouzes[3], Frédéric Moulin[3], Nicole Goutal[4], Marina Oukacine[4,1], Yann Peltier[4], Rui M.L. Ferreira[5], Moisés Brito[5], Elsa Alves[6], Miltiadis Gymnopoulos[6], Joao Leal[7], Bastien Mathurin[8], Sandra Soarez-Frazao[8], Didier Bousmar[9], Joao Fernandes[10], and Olivier Eiff[11]

[1]*Irstea, Unité de Recherche Hydrologie-Hydraulique, 5 rue de la Doua CS70077 69626 Villeurbanne cedex, France.*
[2]*Laboratoire de Mécanique des Fluides et d'Acoustique, 20 av. A. Einstein, 69621 Villeurbanne Cedex, France*
[3]*Institut de Mécanique des Fluides de Toulouse, 2 allée du professeur Camille Soula, 31400 Toulouse, France*
[4]*Laboratoire d'Hydraulique Saint-Venant (LHSV), 6 quai Watier, BP 49 78401 Chatou*
[5]*CERIS, Instituto Superior Técnico, Universidade de Lisboa,1 av. Rovisco Pais, CP 1049-001, Lisbon, Portugal*
[6]*Laboratorio Nacional de Engenharia Civil, 101 Av. do Brasil, CP 1700-066, Lisboa, Portugal*
[7]*Universitetet i Agder,Jon Lillietunsvei 9, CP 4879, Grimstad, Norway*
[8]*Université catholique de Louvain, 1 bte L.05.01, Place du Levant, CP 1348, Louvain-la-Neuve, Belgium*
[9]*Service Public de Wallonie, SPW-DO.222, 164 rue de l'Abattoir, 6200 Châtelet, Belgium*
[10]*Eidgenössische Technische Hochschule Zürich, Zurich, Switzerland*
[11]*Karlsruher Institut für Technologie, Karlrühe, Germany*

Abstract. Flood hazards (flow depth and velocity) must be accurately assessed in high-risk areas during extreme flood events. However, the prediction of the very high flows is not an easy task due to the lack of field data and to the strong link between flow resistance and the land occupation of the floodplain. Confinement and inhomogeneity in lateral and longitudinal directions of hydraulic roughness strongly vary with return period T. The physical processes are complex, some still largely unexplored, and the assumptions linked to numerical modelling cannot be validated without field data. The FlowRes project (2015-2018), funded by the French National Research Agency (ANR), aims at improving the flood hazard assessment in floodplains in: 1) investigating in laboratory the hydrodynamic structure associated with extreme flood flows for various land occupations and flow discharge magnitudes; 2) assessing if the existing numerical modelling practices used for $T \sim 100$ years are still valid for extreme events with $T > 1000$ years, relying on the experimental data and on one field case. This paper reports some results obtained during the first year of the project.

1 Introduction

The FlowRes project (2015-2018), funded by the French National Research Agency (ANR), addresses the effect of evolving land occupations (*i.e.* varying Flow Resistance) on extreme flows over the floodplains where vulnerability and risk are located. Both the specific physical processes related to the very high flows and their numerical modeling are handled.

The project focuses on the flow resistance caused by three types of hydraulic roughness elements commonly encountered on floodplains: meadows, trees and houses. Depending on the flow rate magnitude, these roughness elements can be modeled as bed-induced roughness, emergent or weakly submerged macro-roughness.

The project distinguishes two different flow domains: (a) the compound channel, in the case of a strong interaction between the flow in the Main Channel (MC) of the river and the flow in the Floodplains (FP); (b) the FP considered as a single rectangular cross-section channel, in the case of a negligible MC/FP interaction (far from the interface with the MC and/or when the FP flow is mainly driven by the FP roughness elements).

The consortium of the FlowRes project is composed of eleven partners, mentioned above in the affiliations of the co-authors. The project is divided into two main tasks, as shown in Table 1: experiments in laboratory flumes (Task 1), and assessment and improvement of the modelling practices (Task 2). The laboratory experiments focus on the effects on flow structure of: longitudinal and lateral transitions in hydraulic roughness, of the confinement degree of the roughness elements, and of the spatial distribution and density of these elements. The experiments are carried out in five flumes, under uniform or non-uniform flow conditions in the streamwise direction, relying on the state-of-the-art measurements on both large and small scales (*i.e.* the river reach scale or the roughness elements scale). For the second task, the previous experimental database is compared to

[a] Corresponding author: sebastien.proust@irstea.fr

© The Authors, published by EDP Sciences. This is an open access article distributed under the terms of the Creative Commons Attribution License 4.0 (http://creativecommons.org/licenses/by/4.0/).

simulations performed with industrial and research codes (1D to 3D modelling). The classical methods to model flow resistance with an increasing complexity are assessed and improved to capture the physics for the entire span of studied flow rates. The codes and methods are then applied to the floods at Besançon, France. Events with a return period T~100, 1000 and 10000-year are simulated with both classical and improved methods, and the discrepancies will be calculated. This project will permit to quantify uncertainties on water levels and velocities computed for extreme events.

The present paper focuses on the work carried out during the first year of the project (2015), mostly measurements in laboratory flumes and preliminary numerical results.

Task 1: Laboratory experiments	
1.1	Vertical transition in hydraulic roughness from emergence to low submergence of the roughness elements
1.2	Longitudinal transition in hydraulic roughness
1.3	Lateral transition in hydraulic roughness
1.4	Hydraulic roughness of interspersed families of roughness elements
1.5	Combined effects of lateral and longitudinal roughness transitions
Task 2: Assessment and improvement of the modelling practices (1D to 3D)	
2.1	Numerical simulations against experimental data
2.2	Numerical simulations of flood events at Besançon

Table 1. Structure of the FlowRes project: tasks and sub-tasks.

2 Laboratory experiments

2.1 Vertical transition in hydraulic roughness from emergence to low submergence of the roughness elements

The existence of a universal profile for the turbulent boundary layer over a rough bed, especially a log-law profile, has been predicted theoretically and verified by many experiments, at least for flow conditions where the boundary layer thickness is large in comparison with the rough bed geometrical scales. Models to predict the hydraulic roughness k_s have been developed for urban canopies formed of cubic-like roughness elements (see *e.g.* McDonald (2000) [1]), based upon a parametrisation of the drag behind individual roughness elements of height h and of the mixing layer profiles in the canopy (region with elevation $z < h$). This approach also applies to emergent roughness elements. The same framework was applied to plant canopies by Nepf and Vivoni (2000) [2] to model the drag and velocity profiles of canopies formed by very elongated individual roughness elements.

Recently, the question of the persistence of a log-law profile in very confined flow with $h/D<1$ (where D is the flow depth) in the limit $h/D\rightarrow1$ has been addressed by different authors, following the claim by Jiménez (2004) [3] that log-law should disappear for $h/D>0.025$. All agree on the necessity to use the double-averaging methodology proposed by Nikora *et al.* (2007) [4] in order to describe the flow inside the roughness sublayer, but few experiments achieve enough spatial convergence to obtain correct estimates of double-average quantities, as discussed in Florens *et al.* (2013) [5]. Surprisingly, it was found that profiles above the canopy ($z>h$) still exhibit log-law behaviours for values of h/D as large as 0.66, see Rouzès *et al.* (2016) [6].

The experimental study proposed as part of this project aims at performing measurements both above and inside the canopy for flow regimes around the transition between emergent ($h/D>1$) and submerged ($h/D<1$) roughness elements. The measurements must provide both spatially and temporally converged double-averaged flow quantities. The roughness elements shape must allow a comparative study of urban-like canopies (with $h\approx l$, where l is the element width) formed by cubic roughness elements and plant-like canopies formed by elongated roughness elements (with $h>> l$).

2.1.1 Experimental set-up

Experiments are carried out at the Institut de Mécanique des Fluides de Toulouse (IMFT) in a 26-m-long, 1.10-m-wide and 0.50-m-deep open-channel flume with a 13-m-long section made out of glass and a slope of 0.3 %. Water level can be adjusted with a downstream weir. The bottom of the open-channel was filled up with a 10-m-long rough bed placed 10 m after the tranquilization section, in order to obtain both fully developed boundary layer and uniform flow conditions at the centre of the rough bed. The rough bed was formed by 4 cm cubes arranged in square configuration, separated by a distance L=9 cm, yielding a frontal density $\lambda_f=h.l/L^2=0.20$. This configuration is the same as S1 in Eiff *et al.* (2014) [7], except for the length scale l which is doubled.

In the measurement section, glass cubes were used to allow optical access. Longitudinal vertical laser sheets were generated from below through the bottom of the channel, using a special optic system (parallel laser sheet generator) in order to generate a 10 cm wide parallel laser sheet. Almost no shadows were then generated when propagation occurred through the glass cubes. Images were recorded from the flume side, the camera looking through water or an alley of transparent glass cubes. A telecentric lens was used to prevent any parallax. All PIV measurements were performed in vertical planes near the centre of the flume. See Figure 1 for a view of the measurement system.

This set-up allows access to the whole flow region, from z=0 to z=D, as can be seen in Figure 2 (right), with a spatial resolution of 2 mm as inferred from preliminary PIV calculations.

For the more submerged flow regime (h/D=0.24), 9 vertical planes located in the periodic pattern were used (to be compared to the 3 planes used by Florens *et al.* (2013) [5] and Eiff *et al.*, 2014 [7], as shown in Figure 2

(left). Only 5 planes were used for the other flow regimes.

The Table 2 contains the flow regimes investigated with the rough bed of cubes, along with the measurement conditions.

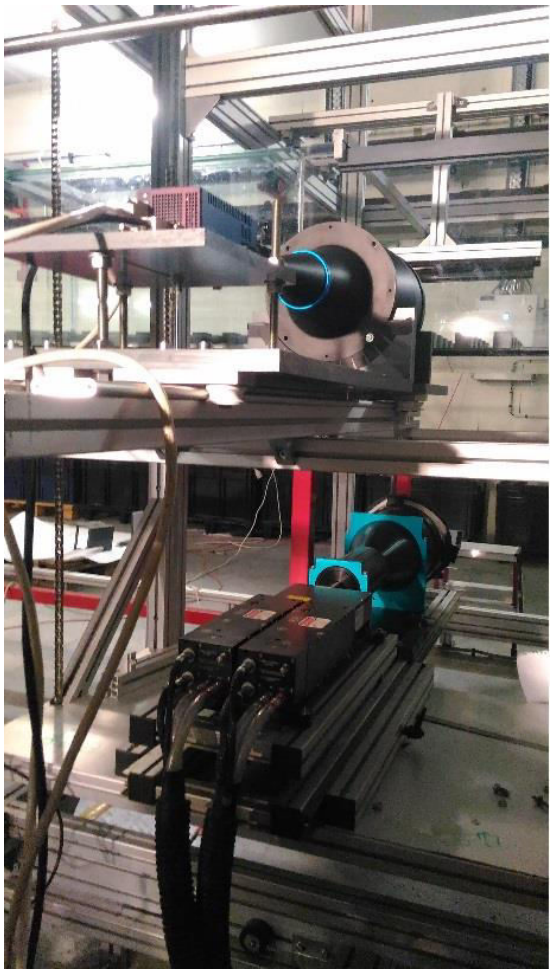

Figure 1. PIV measurement system for measurements inside the canopy. The upper system is the camera with its telecentric lens to avoid any parallax effect. The lower system is a 200 mJ pulsed Nd-Yag laser connected to a parallel laser sheet generator. A 45° inclined mirror reflects the laser sheet vertically through the bottom of the flume.

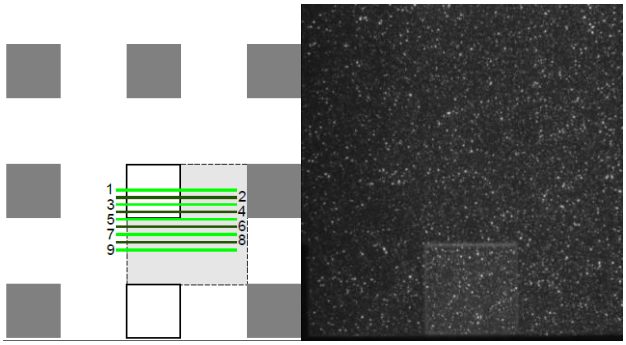

Figure 2. Position of the measurement plane near the centre of the flume (left) and typical image of particles recorded by the camera (right) for plane 9. The specific optical setup shown in Figure 1 allows recording of particles even in the part of the flow that would be hidden by cubes.

Q (L/s)	*D (mm)*	*Fr*	*h/D*	*Np*	*Ni*
90.47	*165.5*	*0.79*	*0.24*	*9*	*10000*
17.99	*80.0*	*0.32*	*0.50*	*5*	*10000*
8.97	*60.0*	*0.22*	*0.66*	*5*	*10000*
5.80	*53.0*	*0.16*	*0.75*	*5*	*10000*
3.96	*44.4*	*0.13*	*0.90*	*5*	*3000*
3.16	*40.1*	*0.11*	*1.00*	*5*	*10000*
2.62	*36.4*	*0.10*	*1.10*	*5*	*3000*
2.37	*32.0*	*0.11*	*1.25*	*5*	*10000*
1.38	*20.0*	*0.10*	*2.00*	*5*	*3000*

Table 2. Experiments in the IMFT flume (sub-task 1.1): flow regimes investigated. Q is the volume discharge, D the water depth, Fr the bulk velocity Froude number, Np the number of measurement plane inside the periodic pattern, and Ni the number of bursts recorded for PIV measurements.

2.1.2 Expected results

Firstly, the measurements for h/D=0.24 will be used to investigate the spatial convergence in the canopy flow region ($z<h$), extending the results of Florens *et al.* (2013) [5] that apply only to the upper flow region ($z>h$).

Secondly, a statistical approach will be used, based upon double average quantities, in order to investigate the transition from submerged to emergent flow conditions. The validity of models developed for vertical velocity profiles for urban or plan canopies will be discussed by comparison with this set of experimental data.

Finally, an analysis of coherent structures will be conducted to study the impact of growing confinement (increasing h/D) on the different contributions for turbulence (namely, following Poggi *et al.* (2014) [8], the linearly growing size of structures above the canopy for $z\geq h$, the shear layer dynamics near $z=h$ and the turbulent wake in the canopy for $z\leq h$).

Moreover, similar experiments for elongated square prisms with h/l=3 and h/l=9 but the same value of L/l will be carried out in the near-future and will complete this first set of experimental data, in order to document the transition from urban-like to plant-like canopy flows.

2.2 Longitudinal transition in hydraulic roughness

2.2.1 From bed-friction to emergent macro roughness drag, or vice versa

In the literature of open-channel flows, the longitudinal transition in hydraulic roughness was experimentally investigated essentially in the case of a transition between two types of bed roughness, see *e.g.* Chen and Chiew (2003) [9]. By contrast, the FlowRes project addresses the issue of a longitudinal change between two different types of hydraulic roughness: bed-induced roughness and emergent macro-roughness. We chose to investigate a flow configuration often encountered in the field, a transition from highly submerged dense meadows to emergent trees, or vice-versa. Similar experiments (same land occupation) are conducted with a single or a compound cross-section, to

highlight the specific role of the MC in the global flow resistance for very high flows. The second objective of Task 1.2 is to combine streamwise non-uniformity of flow with high velocity differences between MC and FP for high overbank flows. This will result in high values of lateral exchange of streamwise momentum caused by both the turbulent mixing and mean flow.

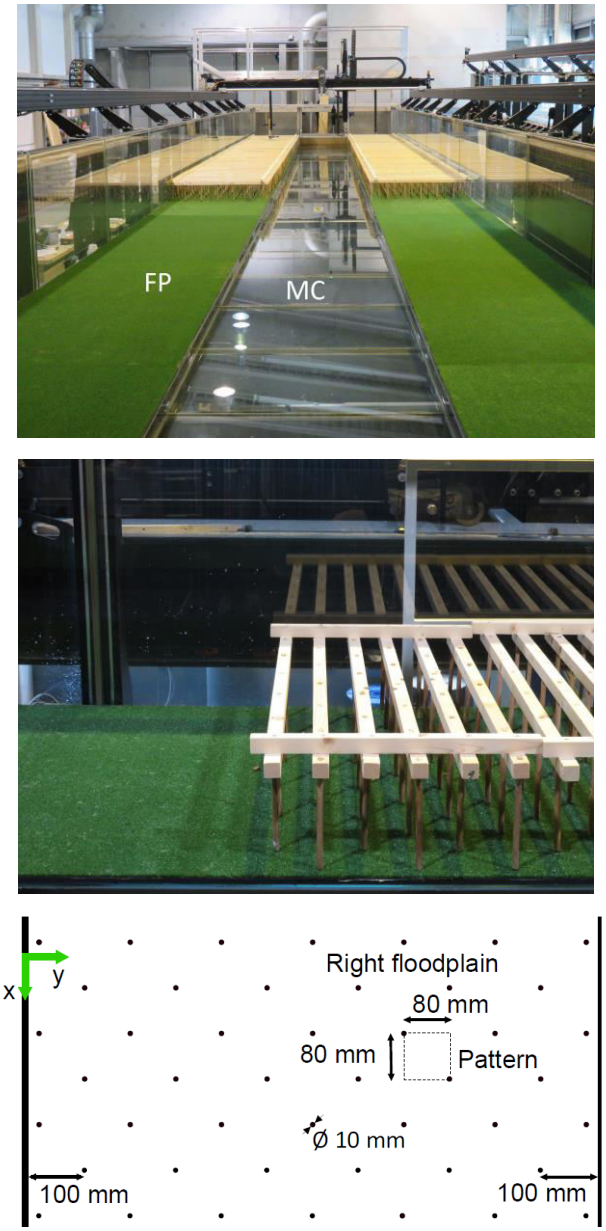

Figure 3. Experiments of Dupuis (2016) [10], sub-task 1.2: (Top) downstream view of the compound channel flume located at Irstea, with a transition Tree-models / Meadow over the FP. (Middle) Side-view of the transition. (Bottom) Top view of the staggered distribution of tree-models.

The experiments were performed by Dupuis (2016) [10] in a flume located at the Institut de Recherche en Sciences et Technologies pour L'environnement et l'Agriculture (Irstea), Lyon-Villeurbanne. The glassed-wall flume (Figure 3) is 18 m long and 3 m wide, with a bottom slope, S_0, of 1.05/1000.

In the case of a compound section, the MC and each of the two 1 m wide lateral FP. The dense meadow over the FP is modeled with artificial plastic grass, whose blades are 5 mm high. The bank full height in the MC is of 115 mm (from MC bottom to the top of the blades of the plastic grass). The emergent trees are modeled by wooden rigid cylindrical stems, with a staggered distribution, as shown in Figure 3 (bottom). The cylinder diameter, ϕ, is of 10 mm, and the stem density, N, is of 81 stems/m².

In the case of a single section, the right-hand FP is isolated from the MC by a vertical sidewall (see Dupuis *et al.* (2015) [11], Dupuis *et al.* 2016 [12]).

Test case	Inlet conditions Q_f (L/s)[1]	Q_m (L/s)	MC flow depth[2] D_m (mm)
Meadow (uniform flow)	18	126	171
Trees (uniform flow)	14	134	214
Meadow / Trees	18	126	211-216
Meadow / Trees	26	110	216-216
Trees / Meadow	12	138	170-161
Trees / Meadow	18	126	184-170

[1] in each FP; [2] for the roughness transitions, variation between the most upstream and downstream measuring sections

Table 3. Flow conditions of the test cases of Dupuis (2016) [10] when the cross-section is compound. Total flow rate Q = 162 L/s.

The flow conditions of the test cases in compound channel are reported in Table 3. The total flow rate, Q, is constant from one test case to another (162 L/s). Two uniform geometries were investigated: the FP is covered over its entire length (18m) either by (1) plastic grass only, or (2) cylinder arrays installed on the plastic grass. In Table 3, the corresponding flow cases are denoted 'Meadow' and 'Trees', respectively. Two non-uniform geometries were investigated: FP with (1) a transition from meadow to trees installed on the meadow (denoted "Meadow / Trees"), or (2) vice versa ("Trees/Meadow"). The change in roughness is located at mid-length of the flume, where the origin of the longitudinal x-axis was chosen (x = 0). In the presence of a roughness transition, the inlet FP discharge, Q_f, was modified as shown in Table 3.

The flow depth was measured with an ultrasonic sensor with an accuracy of ± 0.5 mm (acquisition rate of 50 Hz during 3 minutes). A side-looking ADV probe (Vectrino Plus, Nortek) was used to measure the velocity (acquisition rate = 100 Hz, recording time = 180 s).

Velocity is measured with a lateral step Δy in the range 1 cm to 10 cm (smaller values inside the mixing layer), and with 20 to 25 points for each vertical profile in the MC, or 9 to 13 in the FP.

2.2.2 Flow depth and discharge in the floodplain

We present here some experimental results at the reach scale for the flows in a compound channel with a transition Meadow / Trees and Trees / Meadow (Figure 3-Top). The evolution along the longitudinal direction of flow depth D_f and discharge Q_f in the FP is depicted in Figure 4 (Q_f is calculated by integration of velocity profiles).

The results show that, in the upstream reach (x<0), the flow is strongly driven by the upstream discharge distribution between MC and FP, while in the downstream reach (x≥0), the flow is primarily driven by the downstream water level. In particular, in the upper reach, the lateral mean flow between MC and FP can be enhanced or cancelled depending on the value of FP inflow, denoted $Q_{f\,inlet}$. This may alter the shear-layer turbulence developing at the junction between MC and FP, as previously shown by Proust *et al.* (2013) [13] for non-uniform flows in straight compound channel with smooth FP.

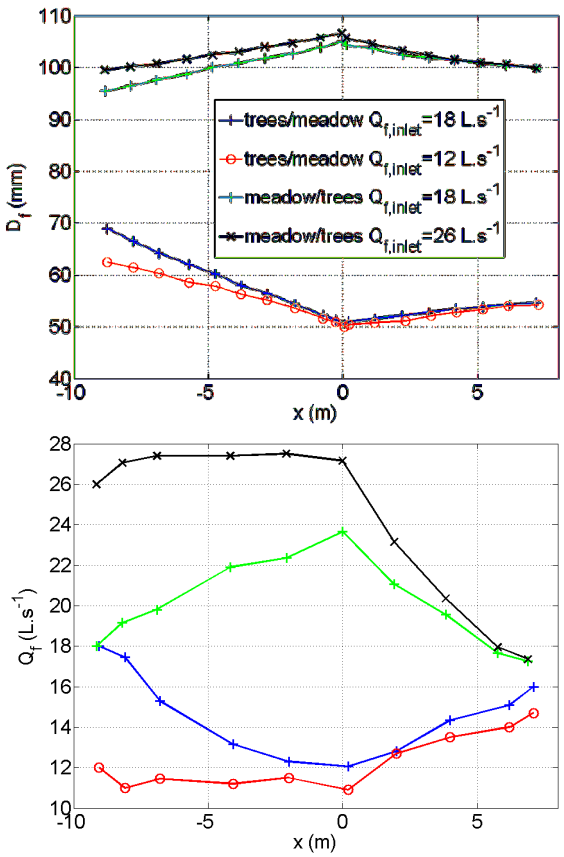

Figure 4. Experiments of Dupuis (2016) [10], sub-task 1.2, compound channel with a longitudinal roughness transition over the FP. Flow depth D_f and discharge Q_f in the FP against downstream position x.

2.3 Lateral transition in hydraulic roughness

The Task 1.3 (Table 1) aims at investigating the flow structure in the case of a lateral transition in hydraulic roughness across the FP. Different land occupations will be examined in the three flumes located at IMFT, Irstea and Laboratorio Nacional de Engenharia Civil (LNEC). Some experimental results obtained at LNEC and IMFT are presented hereafter.

2.3.1 Experiments at LNEC

One of the experiments related to sub-task 1.3 is conducted at Laboratorio Nacional de Engenharia Civil (LNEC), in collaboration with the Instituto Superior Técnico, Lisbon, and Eidgenössische Technische Hochschule Zürich, Switzerland. The experimental work is being carried out in a compound-channel facility (Figure 5 – Top). The channel is a 10 m long and 2 m wide symmetrical compound-channel, comprising a 0.6 m wide and 0.10 m deep MC and two adjacent FP 0.7 m wide. It is made of polished concrete with a bottom longitudinal slope of 0.0011 m/m. The two FP are covered with synthetic grass.

Before the experimental tests with multiple obstacles in the FP, initial tests were conducted to investigate the effects of a single emerging cylindrical obstacle with 5 cm diameter, placed on the middle of the FP, on the characteristic flow processes. 3D instant-velocity recordings are made by means of ADV measurements, with a sample frequency rate of 200 Hz and sampling duration of 180 s, towards the extraction of mean-flow characteristics including the velocity field (Figure 5 - bottom), flow-wise vs span-wise Reynolds Shear Stresses, turbulent intensities and variation of the apparent shear stress at the vertical interface of the abrupt velocity discrepancies. Following this experimental test, 3D structures and momentum-exchange processes at the interface of the MC and the FP will be characterized based on experimental tests with the cylindrical obstacle placed in the interface.

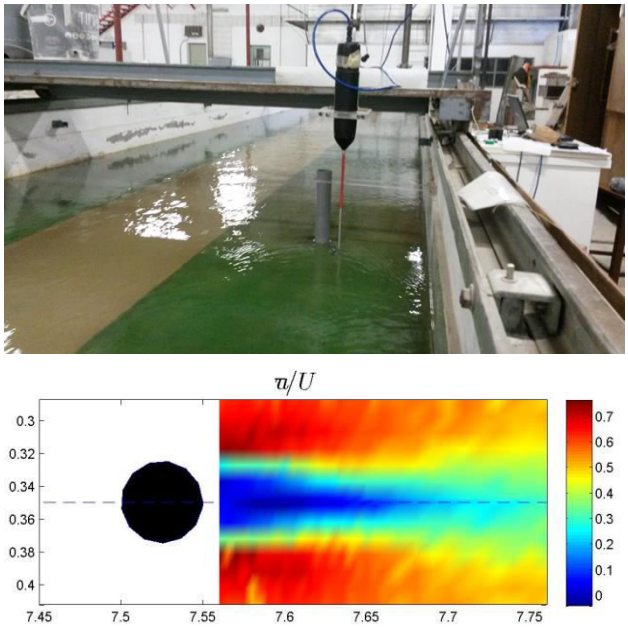

Figure 5. Experiments at LNEC (sub-task 1.3), compound section with dense meadow over the FP: (Top) test with a single circular cylinder; (bottom) normalized mean flow-wise velocity at the wake of a circular cylinder

2.3.2 Experiments at IMFT

Experiments were carried out in the same flume as for the study of the submergence / emergence transition (see section 2.1). The bottom of the open-channel was filled up with a 21.4-m-long rough bed placed 2.60m after the tranquilization section. The half left and right sides of the flume were filled up with 2 cm cubes arranged in respectively staggered and square configurations, with frontal densities λ_f=0.20 and λ_f=0.40 (the configurations S1 and S2 of Eiff *et al.,* 2014 [7]). The roughness discontinuity is then located along the centre of the channel (see Figure 6).

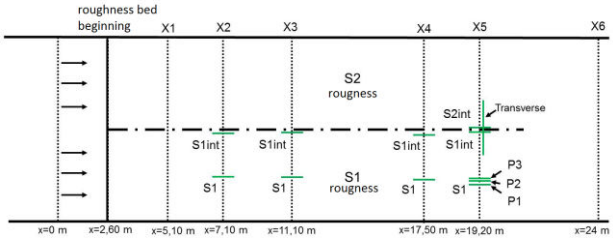

Figure 6. Top view of the flume with positions of the SPIV vertical measurement planes, from Rouzès (2015) [14].

Three different flow regimes were studied, generated with discharge rates Q of around 2.2 Ls^{-1}, 5.4 Ls^{-1} and 15.8 Ls^{-1} in order to reach water depth D equal respectively to 6 cm, 4 cm and 2 cm. These flow conditions yield values of the relative submergence h/D equal respectively to 0.33, 0.5 and 0.66.

Measurements in the centre of the rough bed S1 for completely developed flow conditions (at position X5) were used to investigate the turbulent boundary layer structure above the canopy for high values of h/D, focusing in particular on the roughness sublayer extent and the log law parameters. These measurements and results are analysed in a separate publication (see Rouzès *et al.* (2016) [6]).

Measurements in longitudinal vertical planes near the discontinuity of bed roughness (noted S1int in figure 1) were used to investigate the flow structure at the interface between the two flow regions S1 and S2, and its development along the flume. Stereoscopic measurements give access to the three components of the flow in the laser sheet plane, allowing calculations of the different transverse fluxes of momentum.

Preliminary analysis of the interfacial measurements (namely in S1int planes) show that secondary currents persist deep inside the roughness sublayer even for high values of h/D, as visible in Figure 7.

Stereoscopic PIV measurements in the transverse vertical plane located at X5 (see Figure X) were done at high frequency. Under the frozen turbulence assumption, time-series of $u(y,z,t)$, $v(y,z,t)$ and $w(y,z,t)$ are transformed into a 3D-3C velocity field $u(x,y,z)$, $v(x,y,z)$ and $w(x,y,z)$ providing useful experimental data for coherent structure analysis beside classical statistical approach.

Following Vermaas *et al.* (2011) [15], both sets of experimental data will be used to quantify the contributions of the different processes responsible for the transverse fluxes of momentum: net mass exchanges between the two regions, the presence of a horizontal mixing layer, and the secondary current generated around the discontinuity. The statistical approach will be completed by an analysis of coherent flow structures.

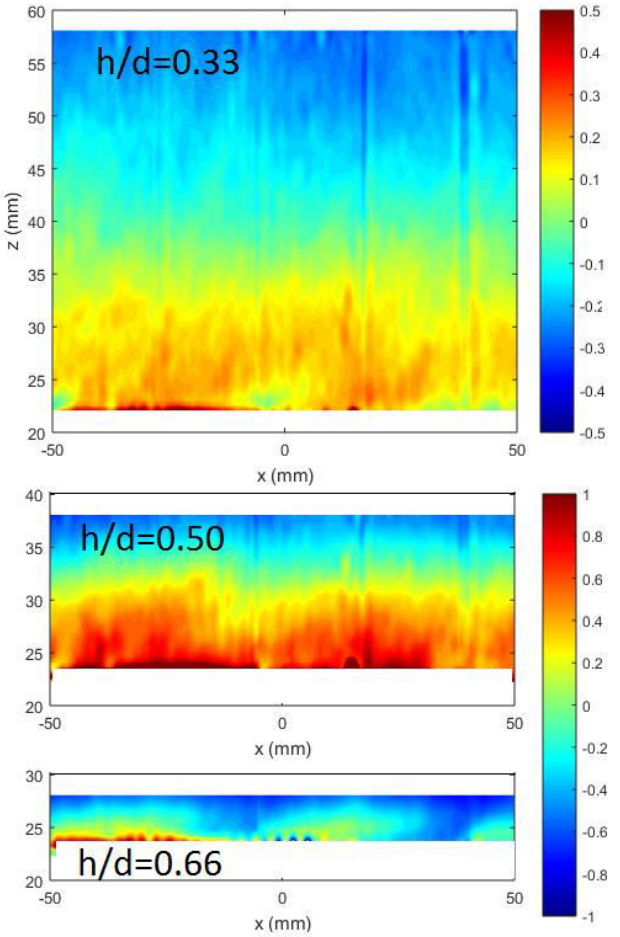

Figure 7. Time-averaged transverse velocity field $V(x,z)$ normalized by friction velocity u^* above the discontinuity (vertical plane S1int at X5 of Figure 6) for decreasing submergence. The flow depth is denoted here d (d=D). The upper color table applies to h/D=0.33 flow regime. The lower color table applies to h/D=0.50 and 0.66 flow regimes.

2.4 Hydraulic roughness of interspersed families of roughness elements

The sub-task 1.4 of the FlowRes project (Table 1) will be dedicated to the study of interspersed families of roughness elements, namely to the interaction between a uniform bed-induced roughness and emerged obstacles.

2.4.1 Emergent roughness elements over smooth and rough beds

Existing studies carried out in smooth beds {Nepf (1999) [16]; Tanino & Nepf (2008) [17]; Herbich & Shulits (1964) [18]} point out the major influence of the spatial density of emergent roughness elements on both the drag and the bed-friction forces and thus, on the overall flow resistance. In addition, Tanino & Nepf

(2008) [17] estimated that, for smooth beds, the bed friction forces represent about 13% of the overall flow resistance, though they pointed out that in rough beds such as natural FP, the contribution of the bed friction to the overall flow resistance may not be negligible.

The experimental study carried out at the Laboratoire de Mécanique des Fluides et d'Acoustique (LMFA) goes beyond the aforementioned studies by presenting an experimental set-up with rough bed and with direct measurements of the drag force acting on the obstacles. This study focuses on complex land occupation with interspersed types of hydraulic roughness. This study evaluates the contributions of bed-induced friction and drag due to emergent macro-roughness to the global flow resistance of a FP. The objective is twofold: (1) to investigate the transition from a resistance generated by the bed-induced friction (modelled as bed roughness) to a resistance governed by obstacles (modelled as drag forces); (2) to perform a sensitivity analysis, estimating the errors made when adding linearly the two contributions (friction + drag forces) without considering any interaction.

2.4.2 Experimental set-up

To address these objectives, this study proposes an experimental setup based on 42 test cases. The experiments are carried out in a 1.20 m width and 8 m long rectangular laboratory flume with a fixed slope of $S_0 = 0.18$ %. The bottom of the flume is covered by an artificial grass layer, onto which the emergent obstacles are placed (Figure 8).

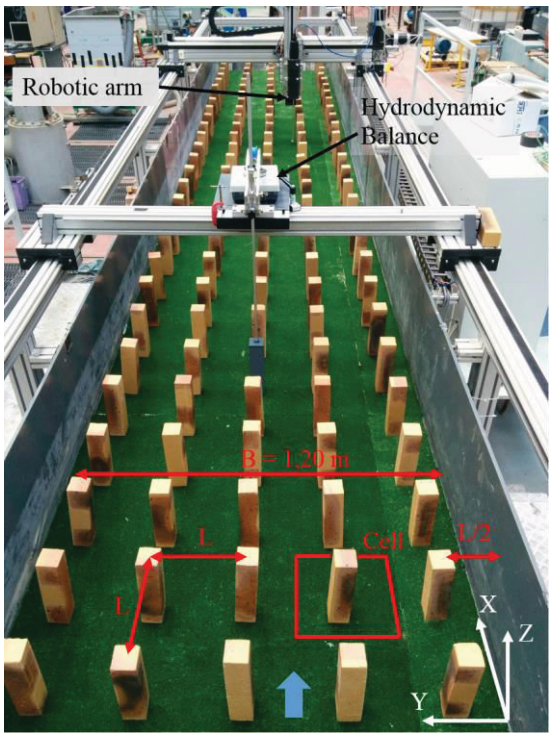

Figure 8. Experiments of sub-task 1.4: downstream view of the laboratory flume located at LMFA.

The obstacles consist of prismatic bricks with dimensions: 0.054 × 0.054 m² along both horizontal directions and remain emergent in all cases. The flume is equipped with a robotic arm that allows displacements in the three directions: *X*, *Y*, and *Z* (Figure 8). This robotic arm allows us to measure water depth by means of an ultrasonic limnimeter and velocities by using a micro-ADV.

In this study, only fully turbulent flows with low Froude number ($Fr < 0.30$) are considered. These considerations allow us to neglect the effects of the Reynolds number (Re) and of the Froude number (Fr), reducing to 4 the number of non-dimensional parameters, namely B/L, λ_f, D/L, and ε/D, where B is the channel width ($B = 1.20$ m), L stands for the distance between the centers of two consecutive obstacles in both directions (X and Y) (Figure 8), the ratio B/L thus denotes the number of bricks per cross-section, ε is the bed roughness height ($\varepsilon = 0.007$ m), and the ratio ε/D denotes the relative roughness. The spatial distribution of the bricks is parameterized by the frontal density $\lambda_f = l.D/L^2$ (emergent elements), with $l = 0.054$ m.

In this study we will consider values of the filling ratio B/L ranging from 5 to 11 (typically 7 cases). For each value of B/L, three values of λ_f and three values of D/L will be studied. Table 4 contains the typical ranges of the different non-dimensional parameters planned in the experiments.

B/L	λ_f	D/L	ε/D
5 to 11	0.15 to 0.25	0.2 to 1.1	0.03 to 0.17

Table 4. Experiments in the LMFA flume (sub-task 1.4): interspersed families of roughness elements. Range of values of the tested parameters.

2.4.3 Expected results

The strategy consists in measuring the drag force F_d that the flow exerts on one obstacle located at the middle of a cell (see Figure 8). Once the value of F_d is known, the bed-friction force F_b can be obtained by applying momentum balance along the streamwise direction and under uniform flow conditions to the measured cell. The momentum balance results in the following expression:

$$F_d + F_b + W = 0 \quad (1)$$

where W stands for the weight component of the water.

Under uniform flow conditions, the drag force F_d is measured by means of a hydrodynamic balance, which is schematized in Figure 9. In this balance the drag force is multiplied by a lever arm whose top end is attached to a weir. This weir pulls a calibrated weight that is on a digital scale, which measures the multiplied force. To determine the point where the drag force acts on the obstacle, each measurement is performed twice by changing the axis of rotation of the lever arm. The drag force F_d is obtained by applying a moment balance around the two axis separately.

Also under uniform flow conditions, water surface and 3D velocity field are characterized in detail for one cell located far enough from boundary conditions (Figure

9). An ultrasonic limnimeter with an accuracy of ± 1 mm is used to measure the water surface and a side-looking Nortek-Vectrino (micro-ADV) is used to measure the 3D velocity field.

The purpose is to obtain the evolution of the ratio F_d / F_b for increasing values of λ_f and D / L. Also, the interaction between bed-friction and drag forces is studied by analysing on the one hand, the influence of the bed friction on the drag coefficient and on the other hand, the influence of the obstacles on the bed-friction coefficient.

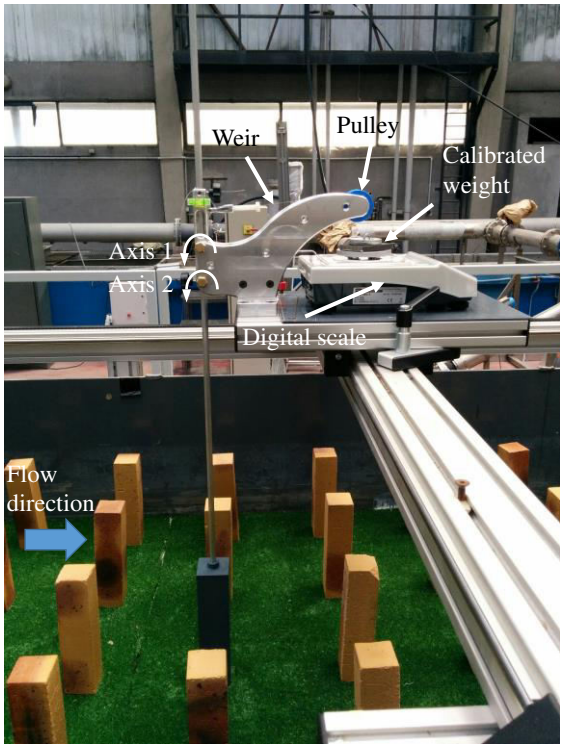

Figure 9. Experiments of sub-task 1.4: lateral view of the hydrodynamic balance.

As a conclusion, this study is expected: (1) to characterize the flow resistance of a FP with varying density of buildings, which represents the increase of human settlement; (2) to quantify the ratio between bed-friction forces and drag forces acting on the flow as the building density increases; (3) to characterize the transition from a flow whose resistance is governed by the bottom friction (for a limited built land occupation), towards a flow whose resistance is governed by the drag forces on buildings (for a high built land occupation).

3 Assessment and improvement of the modelling practices

The second objective of the FlowRes project is to assess if the existing modelling practices that are commonly used for events with return period T up to 100-year are still valid to predict the floodplain flow for $T \geq$ 1000-year. The main stake is to quantify uncertainties on computed water levels and velocities that are directly linked to the modelling of the various contributions to flow resistance. To this end, two different investigations will be carried out.

3.1. Numerical simulations against experimental data

The experimental data related to Task 1 will be compared to simulations with both industrial and research codes (1D, 1D+, 2D and 3D). The aim is twofold: (i) to evaluate the classical methodologies used by practitioners to model the different contributions to flow resistance (Manning-like coefficients, global drag coefficients, porous-media approach, topographic singularity) and (ii) to improve these methodologies to better capture the physics found in the laboratory experiments, irrespective of the return period T. We present here some results using a 1D+ approach, 2D modelling, and 3D modelling with a porous media approach.

3.1.1 1D+ simulation of non-uniform overbank flows with emergent rigid vegetation

The non-uniform flows experimentally investigated during sub-task 1.2 (see section 2.2) were simulated with a 1D+ model called the Independent Sub-sections Method –ISM-, see Proust *et al.* (2016) [19].

The ISM was developed by Proust *et al.* (2009) [20], relying on the works of Yen (1984) [21], Yen *et al.* (1985) [22], and Bousmar & Zech (1999) [23].

The ISM consists in a system of 4 ordinary differential equations (3 momentum and 1 mass conservation equations) that computes the water level and the 3 sub-section-averaged velocities in the right-hand FP, MC and left-hand FP. The ISM is original among the 1D approaches because

- The water surface profile is solved in each sub-section (1D+)
- The sub-section head loss gradients can differ from one sub-section to another ($S_{Hm} \neq S_{Hf}$)
- The actual upstream discharges Q_m and Q_f and the downstream water level can be simultaneously accounted for
- The lateral discharge per unit length q and the depth-averaged lateral Reynolds-stress τ_{int}, at the interface between MC and FP are explicitly computed.

The volume drag force exerted by the stems is modelled by a formula of Nepf (1999) [16]. The head loss in a sub-section i due to drag reads

$$S_i^D = \frac{aC_D U_i^2}{2g} \qquad (2)$$

where U_i = sub-section-averaged mean velocity, the frontal surface per unit volume $a = N\phi = 0.81$ m^{-1}, and C_D = drag coefficient related to each stem.

According to Nepf (1999) [16], the lateral and longitudinal distances between two stems are here (Figure 3 – bottom) such that the interaction between the

cylinder wakes is negligible, resulting in a constant drag coefficient $C_D = 1.2$.

The results of the ISM simulations are shown in Figure 10. Computations are carried out in considering or neglecting the horizontal turbulent mixing between the MC and the FP. The estimate of the flow depth D_f and FP discharge Q_f are in good agreement with the measurements for both the high (Top plot) and the medium (bottom plot) overbank flows. A higher discrepancy is observed for the interfacial Reynolds stress, τ_{int}, but as turbulent mixing is modeled by a simple mixing length model in the horizontal plane, results appear to be satisfactory.

This method is now being developed for field applications (complex geometries, unsteady flows…). The ISM is being implemented in the 1D code MAGE (Irstea Lyon). The simulations work for both inbank and overbank unsteady flows, when considering a unique river reach. The transition between two steady states is also well managed. The next steps are: the comparison with data of Task 1.2; the transition from inbank to overbank flows; and to address the issue of multiple reaches (confluences).

3.1.2 Simulation with Telemac 2D of non-uniform overbank flows with smooth floodplains

Before coping with emergent of weakly submersed roughness elements, some preliminary 2D simulations of overbank flows with smooth FP are being carried out. The experimental data of Proust *et al.* (2013) [13] were used. The compound channel flume is 8m long, 1.2 m wide, with an asymmetrical cross-section (a 0.4m wide MC and 0.8m wide unique FP). The bank full height in the MC is 53 mm with a vertical bank between MC and FP. The non-uniform flows are caused by disequilibrium in the upstream discharge distribution between the MC and the FP.

The simulations are carried out with the open source code TELEMAC 2D. The actual vertical bank is replaced by a sloping bank (horizontal: 50 mm / vertical: 53 mm). The mesh is composed of 2.5-long-edge triangles. A constant turbulent eddy viscosity is used, equal to 0.43×10^{-3} m²/s, which is the depth-averaged value measured by Proust *et al.* (2013) [13] at downstream position x = 5.5 m at the interface MC/FP. At the upstream boundary condition (x = 2.5m), the sub-section-averaged velocities in the MC and FP, U_m and U_f, are imposed and equal to the experimental values. At the downstream boundary condition (x = 7m), a constant water level is imposed (measured value).

A simulation of the lateral distribution of depth-averaged streamwise velocity, U_d, and depth-averaged lateral Reynolds-stress, T_{xy}, at downstream distance x=6.5m (last experimental measuring section) is shown in Figure 11. The results clearly show that the 0th order turbulence model cannot accurately predict the turbulent mixing between the two flows (MC and FP), except the peak Reynolds stress. By contrast, the simulated velocities are in good agreement with the measured ones.

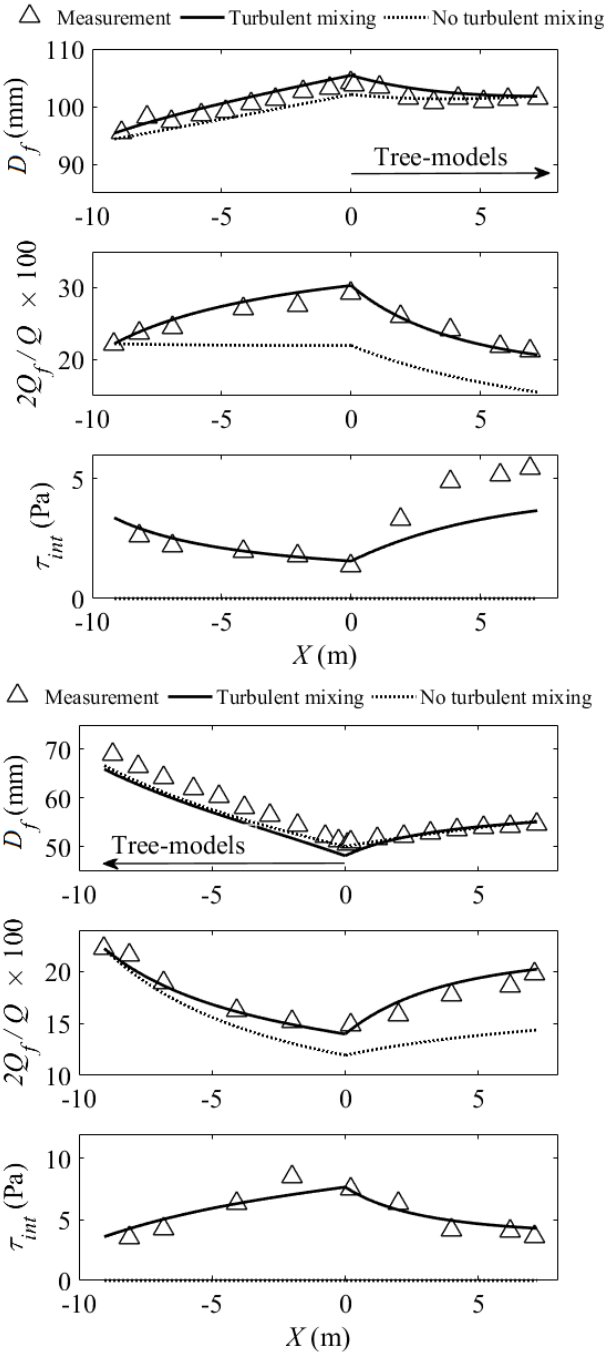

Figure 10. 1D+ simulations (ISM)) against experimental measurements, by considering or neglecting the horizontal turbulent mixing at the interface MC/FP. Longitudinal profiles of flow depth D_f and discharge ratio $2Q_f / Q$ in both FP, and interfacial depth-averaged Reynolds-stress τ_{int}. Test case with FP inflow Q_f = 18 L/s (see Table 3): (Top) transition Meadow / Trees; (bottom) transition Trees / Meadows. Plot taken from *Proust et al.* (2016) [19].

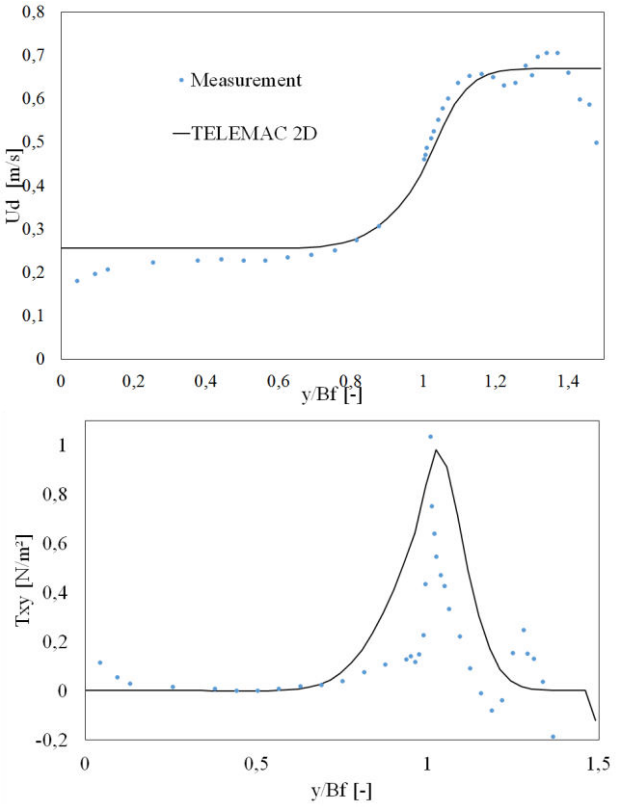

Figure 11. Lateral distribution of depth-averaged streamwise velocity, U_d, and depth-averaged lateral Reynolds-stress, T_{xy}, at downstream distance x=6.5m. The lateral coordinate y is scaled by the FP width, B_f=0.805 m.

3.1.3 3D simulation with porous media approach

An alternative methodology to the drag approach was developed (for more details see Brito *et al.* (2016) [24]) by dividing the flow over vegetated beds in two regions: i) the free-flow above the vegetation layer where a RANS model is used (in the case the Explicit Algebraic Reynolds Stress Model – EARSM, *e.g.* Wallin and Johansson (2000) [25]), and ii) the flow inside the vegetation layer that is modelled as a porous media through a volumetric-average of RANS equations, *e.g.* Whitaker (1999) [26]. On these later equations a source term representing the total drag force per volume unit appears, including both viscous and pressure drag. This term can be estimated by the extended Darcy-Forchheimer model (Li and Ma (2011) [27]):

$$\overline{R}_i = -\frac{\mu\phi}{K}\overline{u}_{D_i} - T\phi\rho\left|\overline{u}_{D_i}\right|\overline{u}_{D_i} \qquad (3)$$

where operators $\overline{\ }$ and $|\ |$ stand for time-averaged and absolute values, respectively, subscript D for Darcy's quantities, ρ and μ is the fluid density and dynamic viscosity, respectively, subscript i represents the i direction, ϕ and K are the porous media porosity and permeability, respectively, and T is the Forchheimer tensor (Li and Ma (2011) [27]). The K and T are estimated from the mean equivalent particles diameter of the vegetation elements, d_{eq}, and the porosity of the porous media using modified Ergun equation (Li and Ma (2011) [27])

$$K = \frac{d_{eq}^2\phi^3}{150(1-\phi)^2} \qquad (4)$$

and

$$T = \frac{1.75(1-\phi)}{d_{eq}\phi^3} \qquad (5)$$

where $d_{eq} = \psi(6V_p/A_p)$, V_p and A_p are the volume and the surface area of the vegetation element, respectively and the shape factor ψ is the ratio between the surface of a sphere of equal volume to the element and the surface area of the vegetation element.

To validate the methodology the model was used to simulate data obtained by Ghisalberti and Nepf (2004) [28] in a rectangular channel using a dense randomly distributed arrange of submerged cylinders. The results for the vertical profiles of the double-averaged streamwise velocity and shear stress (see Figure 12) demonstrate the ability of the model to capture the main features of the flow, namely at the top of the vegetation layer and inside it.

The model was then used in the simulation of compound channel flows with vegetated FP tested at LNEC (Fernandes *et al.* (2014) [29]). The vegetation layer was composed of an artificial grass carpet similar to the one used in Irstea experiments. The results of cross-section distribution of the shear stress for a relative flow depth of 0.30 (see Figure 13) show that (i) the model predicts well the shear in the FP (where the vegetation layer lays) and (ii) the mixing-layer between that sub-section and the MC is relatively well captured.

In view of the encouraging results of the developed porous media methodology, the model will be applied in the simulation of several experiments mentioned in section 2. Namely, its validation will be tested for different vegetation elements geometry (cubes), less dense vegetation and low submerge and emergent vegetation.

3.2. Numerical simulations of flood events at Besançon

In a second time, the numerical models and methodologies used to model flow resistance during the laboratory experiments will be applied to the Doubs River floods at Besançon (located in the Jura mountain of France). The selected area of this field case is a ten kilometres long reach of the Doubs River inside and in the vicinity of the city of Besançon. The urban area was highly flooded in 1910 due to the blockage of wood trunks against two bridges during a rare flood (about 100 year return period for the peak flow). About 45 flood marks were surveyed, which permit (together with testimonies) a quite good description of the flood extent. Data for more recent floods are also available and will

enable a calibration of the flow parameters in the MC of the Doubs river for more usual flow discharges.

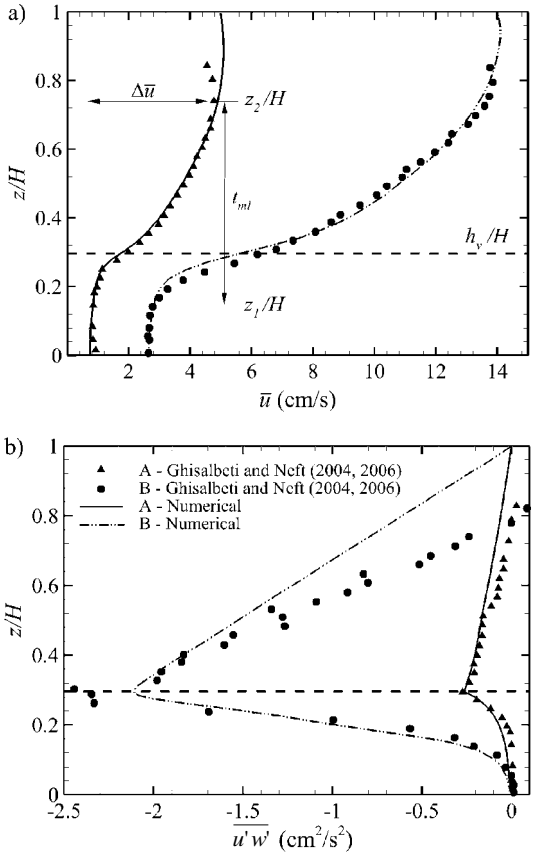

Figure 12. Vertical profiles of double-averaged a) streamwise velocity, and b) shear stresss, for tests A and B of Ghisalberti and Nepf (2004) [28]. The flow depth is denoted here *H*.

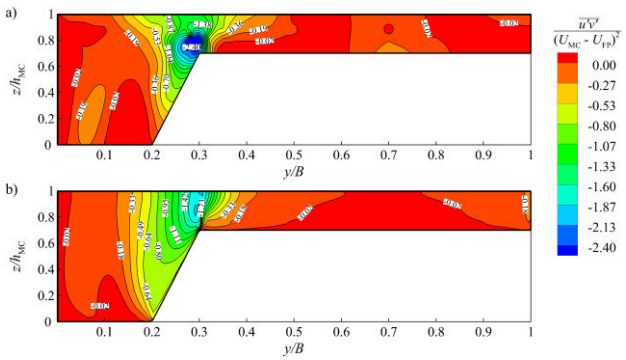

Figure 13. Shear stress field for a relative flow depth of 0.30: a) experimental; b) numerical. The half-width of the flume is denoted here *B*, and the MC flow depth, h_{MC}.

A 2D model using Rubar 20 software will be built in order to be used as reference for comparison with the other models. Calculations will be carried out for the 1910 flood hydrograph and for synthetic hydrographs built to represent the return periods of 10, 100, 1000 and 10 000-year. Land use, hydraulic structures and channel morphology could be defined as the ones in 1910 or the ones in 2010, which will permit to compare the differences due to these changes with the uncertainties due to the modelling parameters

4 Methodological guide on the simulation of extreme floods and experimental data base

The FlowRes project should lead to a valuable tool: a recommendation guide for the numerical simulation of extreme flood flows. This guide will rely on the comparison experimental database / numerical simulations (sub-task 2.1 in Table 1), but also on the simulation of floods at Besancon (sub-task 2.2), to address the issues related to changes in scale from laboratory to field in the high flow context. This guide will be designed for operational users and control authority. It should propose scientific responses to integrate all types of hydraulic roughness encountered in the field, depending on the flow magnitude, the land occupation of the FP, and on the type of numerical modelling (from 1D to 3D). In particular, the uncertainties associated to the different types of flow resistance modelling will be quantified. Lastly, it is also planned to share the experimental data collected during Task 1 in the various flumes with the international scientific community (the database could also be used for benchmarking).

Funding

The FlowRes project is supported by the French National Research Agency (ANR), under grant No ANR-14-CE03-0010.

5 References

1. Macdonald R.W. (2000). Modelling the mean velocity profile in the urban canopy layer. *Bound Layer Meteorol, **97**,* pp. 25–45.
2. Nepf H. and Vivoni E.R. (2000). Flow structure in depth-limited, vegetated flow. *J Geophys Res, **105***, pp. 28547–28557
3. Jiménez J. (2004). Turbulent flows over rough walls, *Annu. Rev. Fluid Mech. **36***, pp. 173–196.
4. Nikora V., McEwan I., McLean S., Coleman S., Pokrajak D. and Walters R. (2007). Double-averaging concept for rough-bed open-channel and overland flows: Theoretical background, *J. Hydr. Eng. 133(8)*, pp. 873–883.
5. Florens E., Eiff O. and Moulin F.Y. (2013). Defining the roughness sublayer and its turbulence statistics. *Exp. Fluids, **54**, 1500.*
6. Rouzès M., Moulin F.Y. and Eiff O. (2016). Effect of relative submergence in rough turbulent open-channel flows. *To be submitted.*
7. Eiff O., Florens E. and Moulin F.Y. (2014). Roughness parameters in shallow open-channel flows. *River Flow 2014*, pp. 287-292
8. Poggi D., Porporato A., Ridolfi L., Albertson J. and Katul G. (2004). The effect of vegetation density on canopy sub-layer turbulence. *Bound. Layer Meteor., **111***, pp. 565–587.

9. Chen, X. and Chiew, Y.M. (2003). Response of velocity and turbulence to sudden change of bed roughness in open-channel flow. *Journal of Hydraulic Engineering*, **129**(1), pp. 35–43.
10. Dupuis V. (2016). Experimental investigation of longitudinal roughness transitions in single and compound channel flows. *PhD Thesis, Université Claude Bernard Lyon 1, Ecole doctorale MEGA*, in preparation.
11. Dupuis, V., Proust, S., Berni, C., Paquier, A., and Thollet, F. (2015). Open-channel flow over longitudinal roughness transition from highly-submerged to emergent vegetation. *E-proceeding of the 36th IAHR World Congress, The Hague, the Netherlands.*
12. Dupuis, V., S. Proust, C. Berni, and A. Paquier (2016), Combined effects of bed friction and emergent cylinder drag in open channel flow, accepted for *Environmental Fluid Mechanics*.
13. Proust, S., J. N. Fernandes, Y. Peltier, J. B. Leal, N. Rivière, and A. H. Cardoso (2013), Turbulent non-uniform flows in straight compound open-channels, *Journal of Hydraulic Research*, **51** (6), 656-667.
14. Rouzès (2015). Etude expérimentale de l'hydrodynamique d'un écoulement turbulent sur fond rugueux en situation naturelle et/ou à faible submersion. *PhD Thesis, INPT-Université de Toulouse*, 182 pages.
15. Vermaas D.A., Uijttewaal W.S.J. and Hoitink, A.J.F. (2011). Lateral transfer of streamwise momentum caused by a roughness transition across a shallow channel. *Water Resources Research*, ***47***, W02530.
16. Nepf, H.M. (1999). Drag, Turbulence, and Diffusion in Flow through Emergent Vegetation. *Water Resources Research,* **35** (2), 479–89.
17. Tanino, Y., and Nepf, HM. (2008). Laboratory Investigation of Mean Drag in a Random Array of Rigid , Emergent Cylinders. *Journal of Hydraulic Engineering,* **134** (January), 34–41.
18. Herbich, J.B., and Shulits, S. (1964). Large Scale Roughness in Open-Channel Flow. *Proceedings of the American Society of Civil Engineers. Journal of the Hydraulics Division*, 203–30.
19. Proust, S., J. B. Faure, V. Dupuis, C. Berni and A. Paquier (2016). 1D+ model for overbank flows with a transition bed friction – emergent rigid vegetation drag. Accepted for *River flow 2016, 8th International Conference on Fluvial Hydraulics, St. Louis, Mo., USA.*
20. Proust, S., D. Bousmar, N. Rivière, A. Paquier and Y. Zech (2009). Non-uniform flow in compound channel: a 1D-method for assessing water level and discharge distribution. *Water Resources Research*, **45** (W12411): 1-16.
21. Yen, B. C. (1984). Hydraulics of flood plains: methodology for backwater computation, *Report of the Institut für wasserbau / Universität Stuttgart*, Wissenschaftlicher Bericht Nr. 84/5.
22. Yen, B. C., R. Camacho, R. Kohane and B. Westrich (1985). Significance of flood plains in backwater computation. *Proc. 21st IAHR Congress, Melbourne, Australia, 19-23 August 1985*, 3: 439-445.
23. Bousmar, D. and Y. Zech (1999). Momentum transfer for practical flow computation. *Journal of Hydraulic Engineering*, **125**(7): 696-706.
24. Brito, M., Fernandes, J. N. and J. B. Leal (2016). Porous media approach for RANS simulation of compound open-channel flows with submerged vegetated floodplains. Submitted to *Environmental Fluid Mechanic*s.
25. Wallin, S. and A. Johansson (2000). A complete explicit algebraic Reynolds stress model for incompressible and compressible turbulent flows. *Journal of Fluid Mechanics*, **403**, 89–132.
26. Whitaker, S. (1999). *The Method of Volume Averaging*. Kluwer Academic Publishers, Dordrecht.
27. Li, L. and W. Ma (2011). Experimental study on the effective particle diameter of a packed bed with non-spherical particles. *Transport in Porous Media*, **89**, 35–48.
28. Ghisalberti, M. and H. M. Nepf (2004). The limited growth of vegetated shear layers. *Water Resources Research*, **40**, W07502.
29. Fernandes, J. N., J. B. Leal, and Cardoso A. H. (2014). Improvement of the Lateral Distribution Method based on the mixing layer theory. *Advances in Water Resources*, **69**, 159–167.